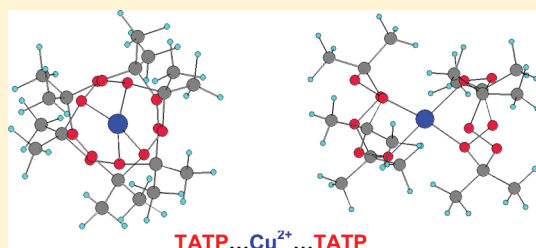


# Role of Metal Ions in the Destruction of TATP: Theoretical Considerations

Faina Dubnikova,<sup>†</sup> Ronnie Kosloff,<sup>†</sup> Jimmie C. Oxley,<sup>‡</sup> James L. Smith,<sup>‡</sup> and Yehuda Zeiri<sup>\*,§,||</sup><sup>†</sup>Institute of Chemistry, Hebrew University, Jerusalem, Israel<sup>‡</sup>Chemistry Department, University of Rhode Island, Kingston, Rhode Island 02881, United States<sup>§</sup>Chemistry Division, Nuclear Research Center—Negev, P.O. Box 9001 Beer-Sheva, 84190 Israel<sup>||</sup>Biomedical Engineering, Ben-Gurion University, Beer-Sheva, 84105 Israel

**ABSTRACT:** The safe decomposition of solid TATP (triacetone triperoxide) explosive is examined theoretically. The route to destruction starts with formation of metal complexes between a metal ion and the TATP molecule. The second step is decomposition of the molecules into stable final products. We examined the structure and stability of both metal ion (including Na<sup>+</sup>, Cu<sup>+</sup>, Cu<sup>2+</sup>, Co<sup>2+</sup>, and Zn<sup>2+</sup>) and proton complexes with TATP using quantum chemical calculations at the DFT-PBE0 level of theory. In addition, for each ion complex, we determined the initial steps in the pathway to decomposition together with the associated transition states. We find that the products of decomposition, in particular, acetone, are also stabilized by ion metal complexes. In agreement with experiment, we find the best candidates for metal ion induced decomposition are Cu<sup>2+</sup> and Zn<sup>2+</sup>.



## I. INTRODUCTION

The chemistry of organic peroxides, which entails the synthesis, characterization, and transformation of derivatives of hydrogen peroxide, has a long history and strong tradition.<sup>1,2</sup> The unusual reactivity of peroxides is generally attributed to weakness of the O–O bond; hence, this is the location where it is homolytically cleaved. Cyclic di- and triperoxides derived from aliphatic ketones are objects of numerous studies related to their application as initiators for the polymerization of vinyl monomers. Unfortunately, in high concentrations, the same materials have explosive properties.<sup>3</sup>

The structures, theoretical details, and properties of TATP and hexamethylene triperoxide diamine (HMTD) have been reported<sup>4–9</sup> as have forensic issues, such as the analysis, detection, stability, and lab-scale destruction.<sup>10–18</sup> Decomposition studies, both experimental and theoretical,<sup>10–18</sup> have been performed at low heating rates (up to 20 K/min) and at isothermal conditions.<sup>19–23</sup> Based on GC/MS results the dominant decomposition product of TATP is acetone, one of the starting materials of TATP synthesis,<sup>20</sup> and calculations by Dubnikova et al.<sup>21</sup> and van Duin et al.<sup>22</sup> confirm this product in the initial reaction pathway.

Terrorist use of peroxide-based explosives such as triacetone triperoxide (TATP) and hexamethylene triperoxide diamine (HMTD; Figure 1), either primaries or the main charge in improvised explosive devices (IED), continues to be of great concern.

For law enforcement agencies, the problems are detection and destruction. These problems are made acute by their extreme sensitivity. Currently, the safest way to dispose illegal explosives is to detonate them on the spot. This procedure safeguards the

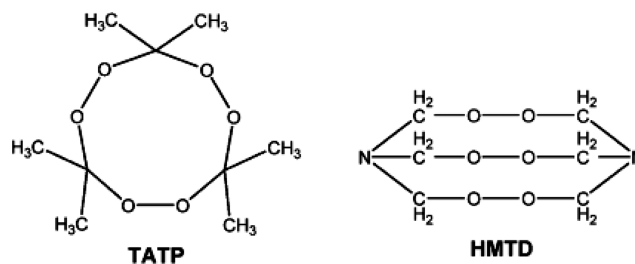


Figure 1. Molecular structures of TATP and HMTD.

law enforcement from handling and transporting these highly sensitive materials. However, in some instances, relatively large quantities (i.e., one kilogram or more) of peroxide explosives are discovered, located in apartments and other high-population density areas. Blow-in-place protocols are impractical in such situations. Hence, there is an urgent need for suitable protocols that will safely destroy large quantities of peroxide-based explosives.

Early work on TATP destruction<sup>16</sup> demonstrated the decomposition of small amounts of TATP using SnCl<sub>2</sub> solutions in water together with organic solvents in an acidic environment. These procedures allowed destruction of TATP in the range of a few grams. In a recent study, the destruction of both TATP and HMTD were examined utilizing various metal ions in acidic water–organic solvent solutions as destroying agents.<sup>24</sup> It has

Received: March 7, 2011

Revised: August 11, 2011

been shown that both  $\text{Zn}^{2+}$  and  $\text{Cu}^{2+}$  ions in tetrahydrofuran (THF) under acidic conditions could lead to complete destruction of TATP and HMTD, but a large excess of ions was required for efficient destruction. Furthermore, destruction of a gram of TATP using concentrated sulfuric acid resulted in an explosion.

To support the experimental efforts to find a mode for gentle destruction of peroxide explosives on the hundreds of gram scale, we initiated a theoretical analysis of the interaction of various metallic ions with TATP. First, we calculated and reported the binding of various metal ions to TATP.<sup>25</sup> These quantum chemical calculations demonstrated that some metal ions bind to the TATP molecules to form complexes in which the TATP structure is not altered. However, a few ions bind to the TATP molecule and lead to destruction of the molecular ring. Other studies demonstrating the importance of the ion–TATP bond include those examining enhanced detection: the  $\text{Na}^+$ –TATP interaction for electrospray ionization<sup>26</sup> and the use of  $\text{Zn}^{2+}$ -doped Titania nanocrystals.<sup>27</sup> The goal of the present work was to unravel detailed chemical decomposition pathways of TATP induced by different ions. It is based on accurate quantum chemical calculations. The calculations incorporate, in an approximate manner, the effect of solvent as well as acid. We believe that this study will provide a rational design of a more efficient and safe destruction method of TATP.

## II. METHOD OF CALCULATIONS

The calculations were carried out using the density functional theory (DFT)-based method, as implemented in the Gaussian 03 package<sup>28</sup> with an appropriate basis set. The PBE1PBE hybrid density functional (also known as PBE0)<sup>29,30</sup> was used in conjunction with the Dunning correlation consistent polarized valence double  $\xi$  (cc-pVDZ) basis set<sup>31</sup> for C, O, H, and Na atoms. Because the bivalent ions ( $\text{Cu}^{2+}$ ,  $\text{Co}^{2+}$ ,  $\text{Zn}^{2+}$ ) have large electron deficiencies we used effective core potential (ECP) in the Christiansen et al. large orbital basis, small core potential (CRENBL ECP).<sup>32–34</sup> The same CRENBL ECP was used in the calculations related to the  $\text{Cu}^+$ –TATP complex. The M06 hybrid functional of Truhlar and Zhao,<sup>35</sup> which is known as an appropriate functional for thermochemical, kinetics, and noncovalent interactions was also employed to carry out the calculations for some of the complexes examined. Comparison between the results obtained by the PBE1PBE and M06 functionals show that the differences in relative energies and in free energies are less than 1.5 kcal/mol. Because the use of the M06 functional is in many cases associated with significant convergence difficulties and a much larger computation time, we used PBE1PBE method in all the calculations reported below. The PBE1PBE functional yield reliable results and is quite economic in the computational time requirements for rather large molecular systems as those discussed below. The structures that had biradical character were located using the unrestricted uPBE1PBE wave function with the destructive  $\alpha$ – $\beta$  and spatial symmetry.

The vibrational analysis of the structures was performed at the same level of theory in order to characterize reliably the optimized structures either as local minima or transition states. All the calculated frequencies, the zero point energies, and the thermal energies correspond to harmonic approximation. The calculations of intrinsic reaction coordinates (IRC) using internal coordinates were performed in order to examine whether the transition states under consideration connect the expected reactants and products. These calculations were performed for all the

transition states at the PBE1PBE level of theory. The basis set used was the same as that used for the stationary point optimizations.

Adducts, consisting of two or more nearly separated species, along the decomposition pathways were identified and localized as local minima on the potential energy surface. The energy associated with these complexes did not include basis set superposition error (BSSE) correction. The value of this correction does not exceed 1 kcal/mol, so for our purpose, it does not have a significant importance.

Implicit solvent effect of the experimental THF (tetrahydrofuran) media has been taken into account via the self-consistent reaction field (SCRF) method using C-PCM polarizable conductor calculation model.<sup>36,37</sup> Gas-phase-like optimized geometries (i.e., molecule without solvent effects) have been used in the single point calculations. In some cases, the full optimization procedure was performed in the solvent and the results compared with those obtained in the solvent-free molecular optimization. In most cases, optimized geometries and energies in the gas-phase-like system and in solvent were in excellent agreement. However, in the case of  $\text{Cu}^{2+}$  optimization in the solvent resulted in a complex where the TATP ring remains closed and has a slightly higher energy than obtained for gas phase optimization.

## III. RESULTS

The first step in the destruction of any solid explosives is its transformation to a molecular form, namely, its dissolution. In the case of TATP, an organic solvent has to be used because the dissolution of TATP in water is very limited. Once the solid is dissolved, the explosive molecules are separated from one another and a chain reaction is much less likely to occur. Moreover, TATP solution is less hazardous to handle because individual molecules are widely separated and evolved heat can be absorbed. The calculations reported below are aimed at the understanding of this second step when metal ions are used to stabilize or transform the TATP molecules to nondetonable species. In a previous study it was shown that metal ions can either form a strongly bound ion–TATP complex or bind to segments of the TATP molecule after the ring shape is destroyed.<sup>25</sup> It is clear that the destruction of TATP and any other peroxide based explosive is associated with major alteration of the molecular structure to form decomposition products that are inert. Hence, a natural pathway to examine is the use of metallic ions that cause destruction of the ring structure upon binding to the TATP molecule.

We carried out a series of thorough quantum chemical calculations aimed at the understanding of the details of the ion–TATP complex formation and decomposition. In general, all the ions considered form stable complexes with TATP. Moreover, these ions tend to reduce the energy barrier required to initiate the decomposition of the complex. In this study we considered the following metallic ions:  $\text{Cr}^{3+}$ ,  $\text{Fe}^{3+}$ ,  $\text{Cu}^+$ ,  $\text{Cu}^{2+}$ ,  $\text{Zn}^{2+}$ ,  $\text{Co}^{2+}$ , and  $\text{Na}^+$ . According to the calculations the first two ions when interacting with TATP open the molecular ring to form spontaneously very stable complexes of the ion bound to three acetone peroxides. We are interested in ions that remain as free ions after the destruction process is over;  $\text{Cr}^{3+}$  and  $\text{Fe}^{2+}$  were not considered farther. All the experimental TATP destruction studies<sup>16,24</sup> were carried out in acidic environments; hence, the complex formed with  $\text{H}_3\text{O}^+$  was also examined. Below we shall describe the interaction of each ion with a TATP molecule and point out the decomposition pathway of the complex. The calculations

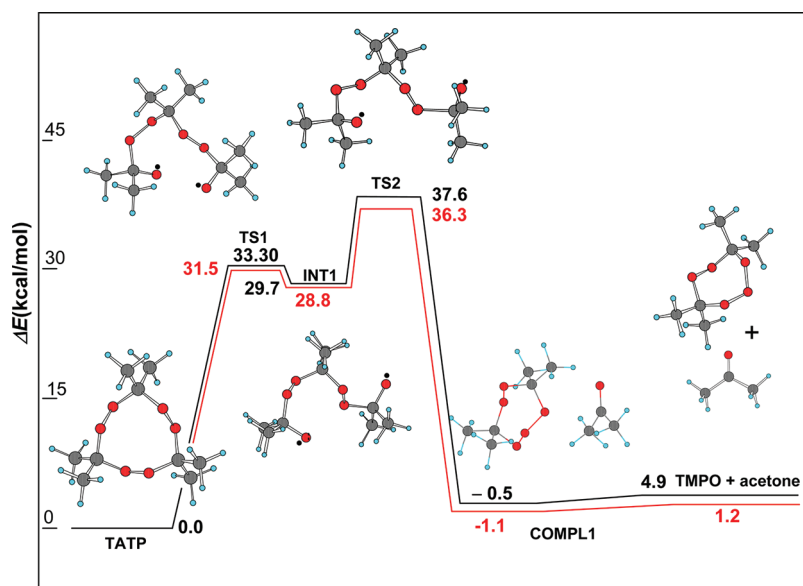


**Figure 2.** TATP decomposition pathway, black line represents an isolated molecule, while red line corresponds to a molecule dissolved in THF. TMPO means 4,4,7,7-tetramethyl-1,2,3,5,6-pentoxepane.

were carried out both for “gas phase” species as well as for solvated systems (see detailed description in the previous section).

**1. TATP.** We start with a short description of the decomposition pathway of a single TATP molecule. The initial stages of the decomposition are shown in Figure 2. The black lines show the decomposition of a single isolated TATP molecule while the red line represents the same process when the TATP is dissolved in tetrahydrofuran (THF).

Inspection of these results shows that the initial step in isolated TATP decomposition requires overcoming an energy barrier of 37.6 kcal/mol. This transition state (TS1) is associated with the opening of a peroxide bond. Once the system passed TS2 the molecule decomposes into an acetone molecule and the remaining fragment forms a seven member ring. The existence of a solvent does not change these steps substantially. The magnitude of TS1 and TS2 is slightly reduced but the structures and decomposition products remain the same. The results shown in Figure 2 agree well with those published in the past<sup>21</sup> with small changes in the numerical values of TS1 and TS2 that are due to the use of a different functional in the present study.

**2. Cu<sup>+</sup>–TATP Complex.** The interaction between a Cu<sup>+</sup> ion and a TATP molecule leads to the formation of a stable complex. The decomposition pathway is shown in Figures 3 (initial decomposition stages) and 4 (late decomposition stages).

Inspection of these results shows that formation of the ion–molecule complex lead to a marked reduction in the magnitude of the energy barrier associated with the first step in the decomposition process as compared to the free TATP molecule. The inclusion of solvent leads to a small additional reduction in the barrier size of about 10%. The initial decomposition step is still associated with rupture of a peroxide bond followed by a rearrangement of the molecular structure to form intermediate (INT1). It should be noted that the energy scale is related to the energy of Cu<sup>+</sup>–TATP complex whose energy is 66 kcal/mol below that of Cu<sup>+</sup> + TATP. Thus, the binding energy of the copper ion to the TATP molecule is 66.2 kcal/mol in the gas phase and reduces to 36.2 kcal/mol for the dissolved complex in THF. The large influence of the THF solvent on the ion–molecule

binding is mainly due to the stabilization of the ion by the solvent molecules defined by eq 1

$$\Delta E_{\text{complex(gasphase-solvated)}} = 6.6(\Delta E_{\text{of TATP}}) + 65.0(\Delta E_{\text{of Cu}^+}) - 41.7(\Delta E_{\text{of TATP-Cu}^+ \text{ complex}}) \quad (1)$$

where  $\Delta E_{\text{complex(gas phase-solvated)}} = 29.9$  [kcal/mol].

The intermediate undergoes further rearrangements that are related to two relatively low energy barriers (TS2 and TS3) followed by a large energy release when the Cu<sup>+</sup> is bound to an eight-member ring on one side and to an acetone molecule in the other side (INT2). The C–O bond opening via TS3 results in some Cu peroxide–three-member ring (Cu–O–O) in INT3 and –O–(CH<sub>3</sub>)<sub>2</sub>C–O–O–C(CH<sub>3</sub>)<sub>2</sub> fragment formation. The next O–O bond rupture leads to the elimination of an acetone molecule (TS4), together with the insertion of a methyl group into the neighboring O–O bond. Thus, instead of the –Cu–O–(CH<sub>3</sub>)<sub>2</sub>C–O–O–C(CH<sub>3</sub>)<sub>2</sub> fragment seen in INT3, we observe the fragment –Cu–O–(CH<sub>3</sub>)C–O–CH<sub>3</sub> and acetone molecule in COMPL1–Cu<sup>+</sup>. Endothermic behavior of the COMPL1–Cu<sup>+</sup> complex to acetone ejection is much lower in the solvent than that in gas phase (i.e., 10.5 compared to 20.5 kcal/mol).

**3. Na<sup>+</sup>–TATP Complex.** The interaction between a Na<sup>+</sup> ion and a TATP molecule leads to the formation of a stable complex whose decomposition route is shown in Figure 5. Inspection of these results shows that formation of the ion–molecule complex leads to a reduction in the magnitude of the energy barrier associated with the first step in the decomposition process of a TATP molecule. The reduction in the barrier height is similar to that obtained in the case of Cu<sup>+</sup>. The inclusion of solvent leads in this case to a small increase in the barrier size of TS1 and to a much larger increase for TS2 of about 30%. This different behavior of Na<sup>+</sup> as compared to Cu<sup>+</sup> is solvent-dependent. The initial decomposition step, TS1, is still associated with rupture of a peroxide bond followed by a rearrangement of the molecular structure to form INT1 followed by TS2. Note that in THF the stability of INT1 is much lower than that in the gas phase. It should be noted

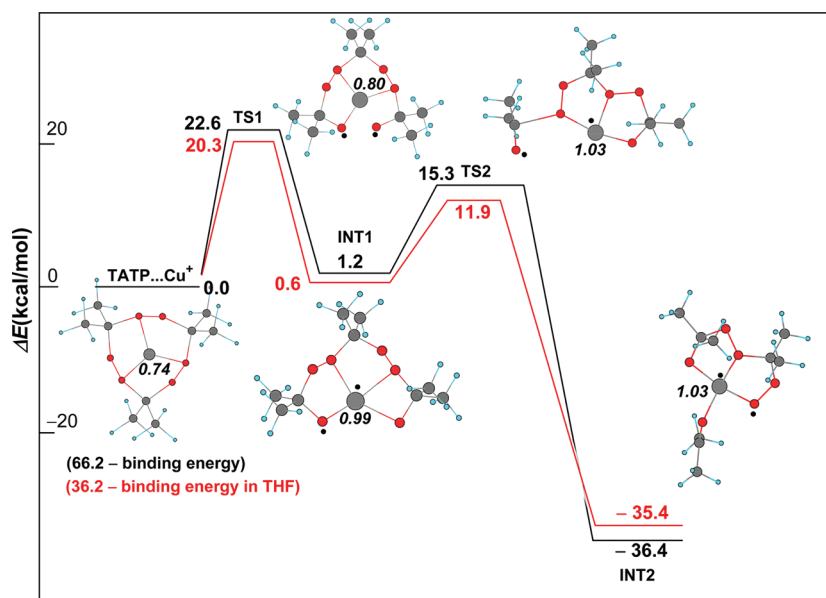


**Figure 3.** Initial stages of  $\text{Cu}^+$ –TATP complex destruction pathway. The symbol  $\bullet$  represents the point of maximum spin density. The charge value (Mulliken) on Cu is presented by bold italic font. Black line shows the decomposition of a gas phase complex, while the red line shows the complex in THF.

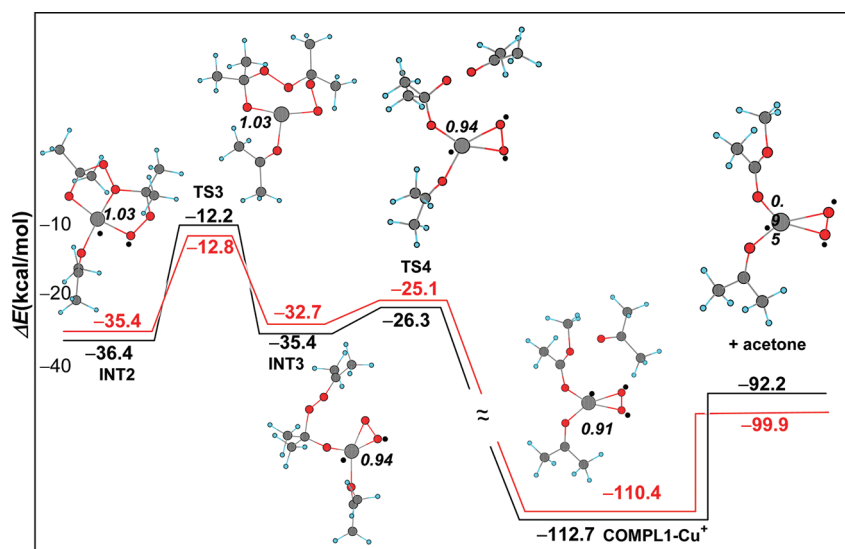


**Figure 4.** Late stages of  $\text{Cu}^+$ –TATP complex destruction until the first acetone molecule is formed. The symbol  $\bullet$  represents the point of maximum spin density. The charge value (Mulliken) on Cu is presented by bold italic font. Black line shows the decomposition of a gas phase complex, while the red line shows a complex in THF.

that the energy scale is related to the energy of  $\text{Na}^+$ –TATP complex whose energy is 45.2 kcal/mol below that of gas phase  $\text{Na}^+$  + TATP and 9.1 kcal/mol below that of the solvated complex. Following TS2 there is further rearrangement to the second intermediate (INT2) in which the Na ion is part of a guarded eight-member ring on one side and bound to an acetone molecule in the other side. The deviation from the  $\text{Cu}^+$  pathway is related to the fact that  $\text{Na}^+$  has no possibility of forming multiple bonds with oxygen as transition metals can. The intermediate INT2 in  $\text{Na}^+$  pathway is much less stable than INT2 in the case of  $\text{Cu}^+$ . The formation of a free acetone molecule and an eighth member ring radical requires investment of less energy than in the case of  $\text{Cu}^+$  (approximately 11 compared to 21 kcal/mol in

gas phase complexes and about 4 and 10 kcal/mol, respectively, in THF). The formation of a free acetone molecule and an eight-member ring radical is the end of the first stage of the complex decomposition.

**4.  $\text{Cu}^{2+}$ –TATP Complex.** The interaction between a  $\text{Cu}^{2+}$  ion and a TATP molecule leads to the formation of a stable complex whose decomposition pathway is shown in Figure 6. Inspection of these results shows that formation of the ion–molecule complex leads to a large reduction in the magnitude of the energy barrier associated with the first step in the decomposition process of the complex. The reduction in the barrier height in this case is larger than that observed for the singly charged ions described above. The inclusion of solvent leads here to an increase in the barrier

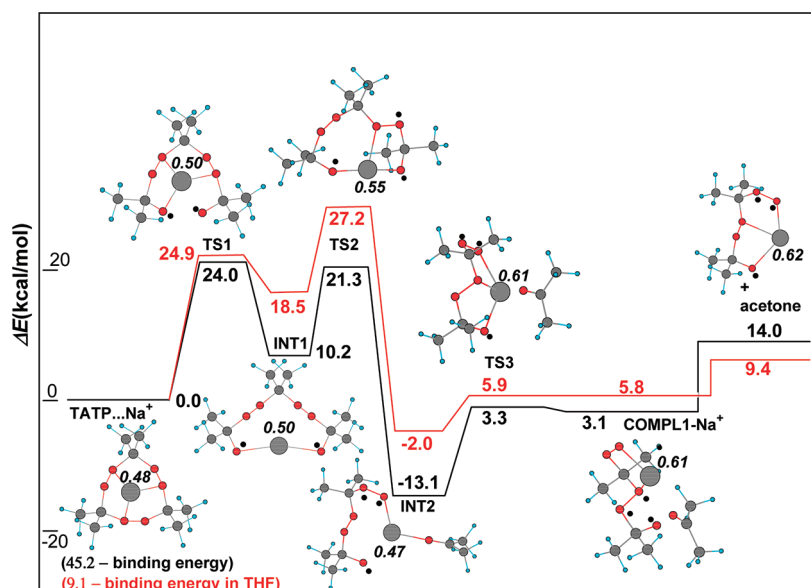


**Figure 5.** Initial stages of  $\text{Na}^+$ –TATP complex destruction pathway. The symbol • represents the point of maximum spin density. The charge value (Mulliken) on Na is presented by bold italic font. Black line shows the decomposition of a gas phase complex, while the red line shows a complex in THF.

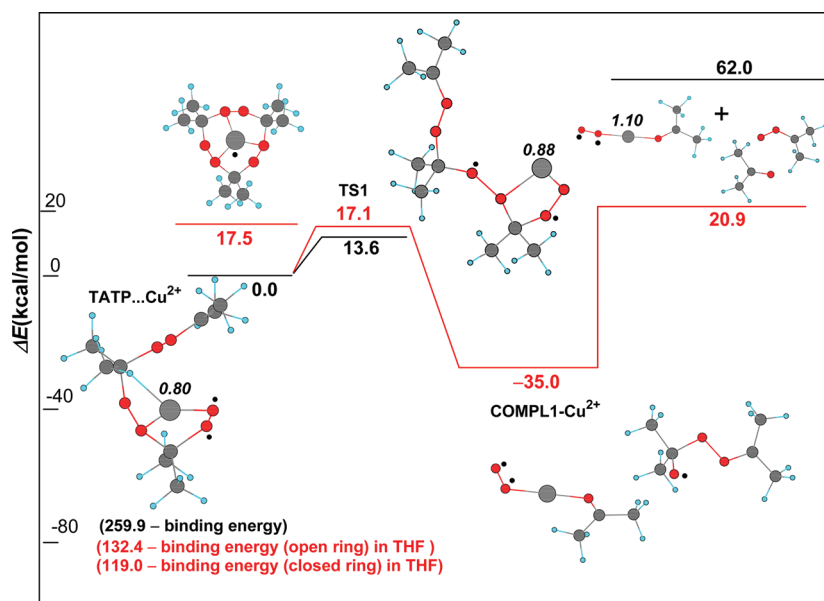


**Figure 6.** Stages in  $\text{Cu}^{2+}$ –TATP complex destruction. The symbol • represents the point of maximum spin density. The charge value (Mulliken) on Cu is presented by bold italic font. Black line shows the decomposition of a gas phase complex, while the red line shows a complex in THF. For the gas phase complex, no stable intermediate species could be identified between TS1 and the decomposition products, hence, such a state is missing in the figure.

magnitude of TS1 of about 25%. Another difference is that two stable species are formed upon binding of  $\text{Cu}^{2+}$  to TATP, a configuration where the metal ion is bonded to the whole molecule above the center of the TATP ring and the other that corresponds to binding of the ion to the TATP after one of the C–O bonds was ruptured. These two forms correspond to slightly different bond strengths (see Figure 6). Comparison between the ion–TATP binding in the gas phase and in the dissolved phase shows that existence of the THF solvent leads to a marked reduction in the binding energy, mainly due to the

stabilization of the ion by the solvent. This difference is calculated using eq 2

$$\Delta E_{(\text{gas phase-THF})} = 6.6(\Delta E_{\text{in TATP}}) + 258.6(\Delta E_{\text{in Cu}^{2+}}) - 143(\Delta E_{\text{in TATP-Cu}^{2+} \text{ complex}}) \quad (2)$$

thus,  $\Delta E_{(\text{gas phase-THF})} = 122.3 \text{ kcal/mol}$ .

The initial decomposition step, via TS1, is followed in this case by a large energy release, while  $\text{COMPL1-Cu}^{2+}$  is formed. The separation of the decomposition products is an endothermic

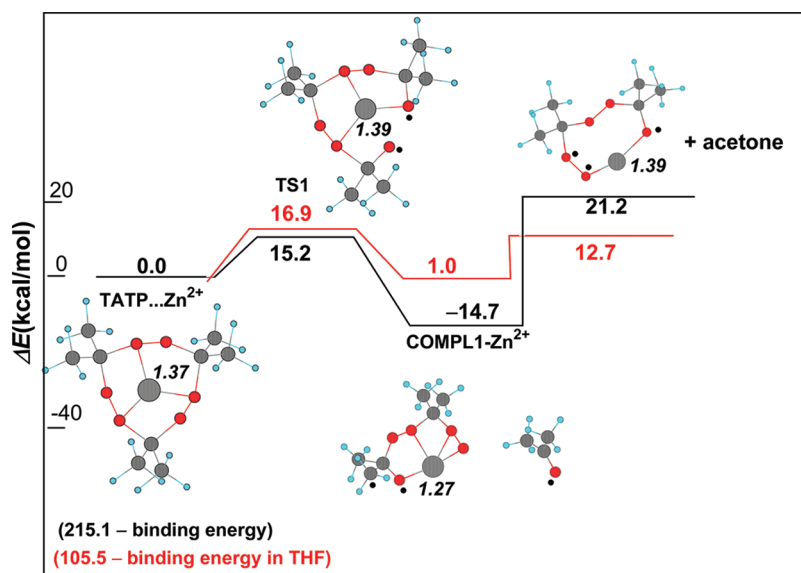


**Figure 7.** Stages in  $\text{Zn}^{2+}$ -TATP complex destruction. The symbol • represents the point of maximum spin density. The charge value (Mulliken) on Zn is presented by bold italic font. Black line shows the decomposition of a gas phase complex, while the red line shows that of a complex in THF.

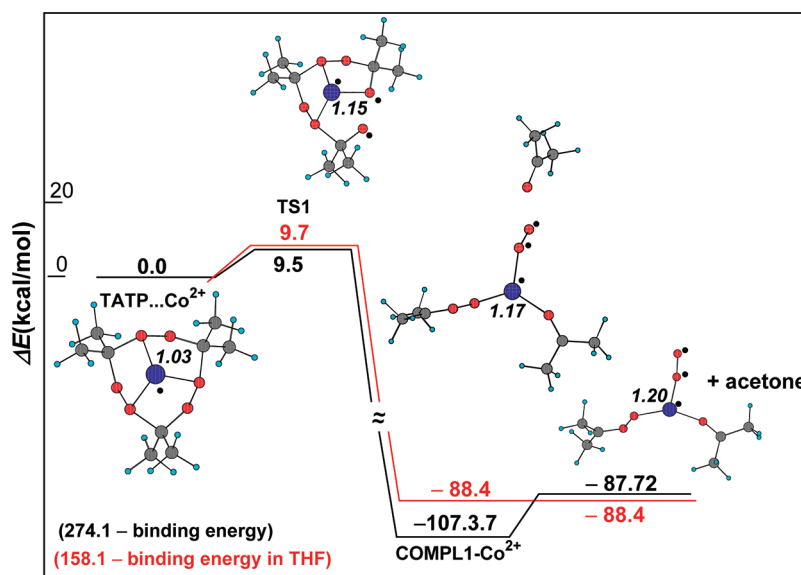


**Figure 8.** Stages in  $\text{Co}^{2+}$ -TATP complex destruction. The symbol • represents the point of maximum spin density. The charge value (Mulliken) on Co is presented by bold italic font. Black line shows the decomposition of a gas phase complex, while the red line shows that of a complex in THF.

process. The final products obtained in this part of the decomposition route are an acetone molecule, an acetone peroxide, and an acetone bonded to the metal ion on one side with a peroxide on the other side of the ion. It should be noted that there is a very large difference in the endothermicity of this last stage when comparing gas phase and solvated systems. The decomposition in THF corresponds to a much lower endothermicity value (see Figure 6).

**5.  $\text{Zn}^{2+}$ -TATP Complex.** The interaction between a  $\text{Zn}^{2+}$  ion and a TATP molecule leads to formation of a stable complex; its decomposition pathway is shown in Figure 7 below. The formation of the ion-molecule complex leads to a large reduction in the magnitude of the energy barrier associated with the first step in the decomposition process of the complex. The reduction in the barrier height is larger than that observed for the singly

charged ions and similar to that observed for  $\text{Cu}^{2+}$ . The inclusion of solvent leads, to a small increase of the energy barrier corresponding to TS1. Comparison between the ion-TATP binding in the gas phase and in the dissolved phase shows that existence of the THF solvent leads to a marked reduction in the binding energy, mainly due to the stabilization of the ion by the solvent. This is similar to the stabilization of  $\text{Cu}^{2+}$ . This difference is clearly seen in Figure 7.

The initial decomposition step, via TS1, is followed by a much smaller energy release while in  $\text{COMPL1-Zn}^{2+}$ . Here too the separation of the decomposition products is endothermic. The final products obtained in this part of the decomposition pathway are an acetone molecule and an eight-member ring species that contains the metal ion. It should be noted that the difference in

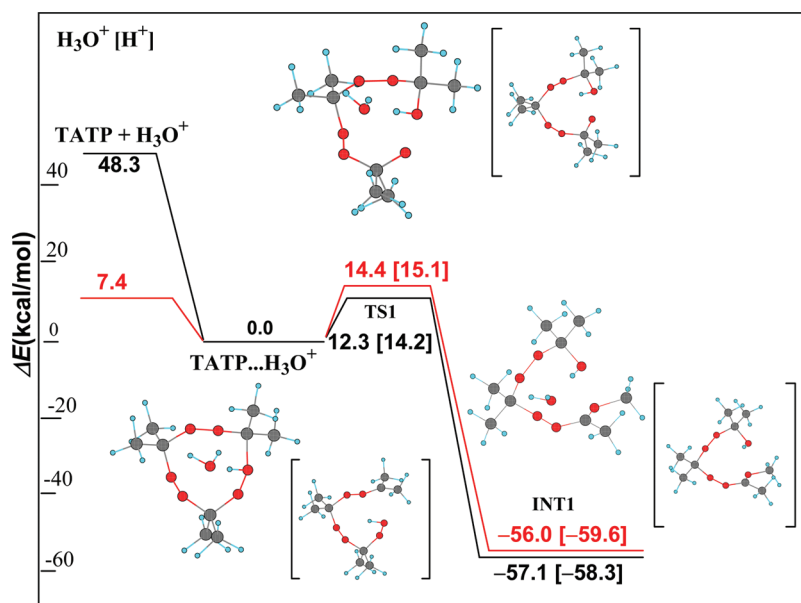


**Figure 9.** Stages in  $\text{H}_3\text{O}^+ - \text{TATP}$  and  $\text{H}^+ - \text{TATP}$  complexes destruction. The symbol  $\bullet$  represents the point of maximum spin density. Black line shows the decomposition of a gas phase complex, while the red line shows that of a complex in THF. Values in brackets represent the  $\text{H}^+ - \text{TATP}$  decomposition pathway.

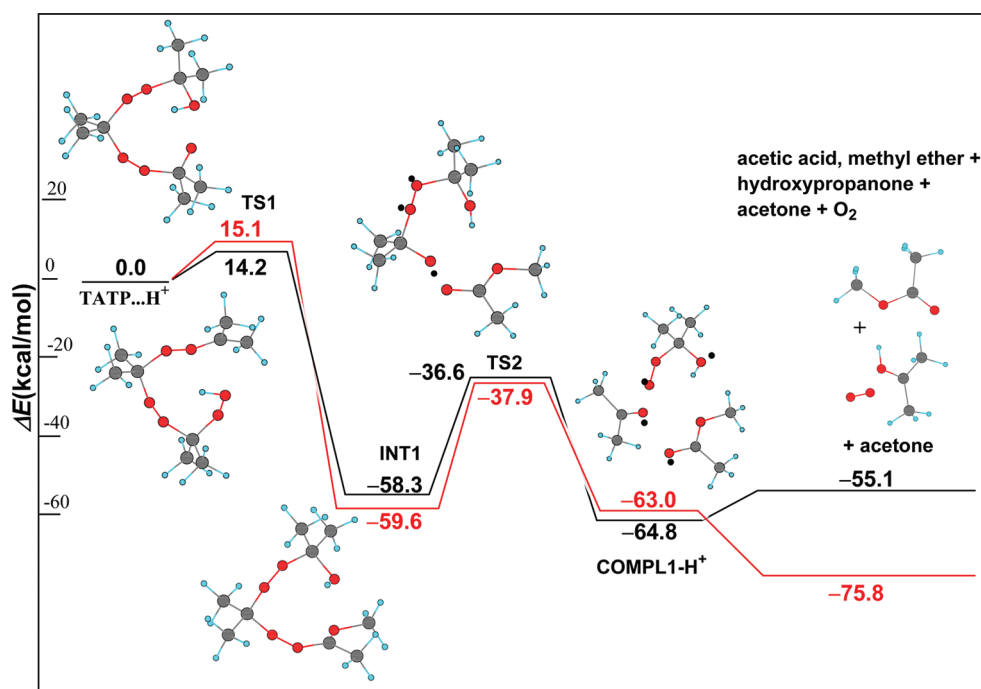


**Figure 10.** Stages in  $\text{H}^+ - \text{TATP}$  complex destruction. The symbol  $\bullet$  represents the point of maximum spin density. Black line shows the decomposition of a gas phase complex, while the red line shows that of a complex in THF.

the endothermicity of this last stage when comparing gas phase and solvated systems is reduced for  $\text{Zn}^{2+}$  as compared to  $\text{Cu}^{2+}$ . The decomposition in THF corresponds to a lower endothermicity value, see Figure 7.

**6.  $\text{Co}^{2+} - \text{TATP}$  Complex.** The interaction between a  $\text{Co}^{2+}$  ion and a TATP molecule leads to the formation of a stable complex whose decomposition pathway is shown in Figure 8 below. The formation of the ion–molecule complex leads to a marked reduction in the magnitude of the energy barrier associated with

the first step in the decomposition process of the complex. The reduction in the barrier height is larger than that observed for the ions discussed above. The inclusion of solvent, in this case, does not alter the magnitude of the energy barrier associated with TS1. Following TS1, one of the O–O bonds opens and an acetone molecule starts to separate from the rest of the complex. This step is associated with a large energy release on the order of 100 kcal/mol. The exothermicity of the first stage in the decomposition process, once the acetone separates from the metal

containing the intermediate biradical, is about 90 kcal/mol. This value seems to be independent of the existence of the THF solvent.

**7.  $\text{H}_3\text{O}^+$ –TATP Complex.** Because the experimental studies were performed in highly acidic environments,<sup>16,24</sup> we examined the complexes formed between TATP and a proton. The complex formed between  $\text{H}^+$  and a TATP molecule is compared to that formed with  $\text{H}_3\text{O}^+$  and TATP in Figures 9 and 10. As demonstrated in Figure 9, the  $\text{H}_3\text{O}^+$  binds to the molecule above the center of the TATP ring by a strong bond in the gas phase that is reduced by a factor of approximately 7 in the solvent. In contrast, inspection of Figure 10 shows that the proton binds to the TATP molecule at one of the oxygen atoms of a peroxide bond following a rupture of a C–O bond. Hence, the  $\text{H}^+$ –TATP complex has a structure in which the molecular ring opens. The structure obtained in this case is basically identical to the TS1 in the case of the  $\text{H}_3\text{O}^+$ –TATP complex, Figure 9. The additional steps to complete the decomposition process for both ions are to a good approximation identical. The magnitude of the energy barrier leading to TS1 (see Figure 9) is very small and it increases by about 15% when a solvated complex is considered. Similar to the case of  $\text{Cu}^{2+}$ , following TS1 there is a large energy release during relaxation of the structure in the intermediate INT1. The

amount of energy release is clearly seen in Figures 9 and 10. The steps in the decomposition process following this relaxation step are shown in Figure 10.

Rupture of a peroxide bond proceeds in a second transition state structure (TS2) that is a precursor to further decomposition into a complex that is constituted from an acetone molecule and two smaller radicals. The separation of the decomposition products constitutes an endothermic process. The final products obtained at the end of this part of the decomposition path are an acetone molecule, an oxygen molecule, a hydroxypropanone and acetic acid methyl ester. The separation of these decomposition products is slightly endothermic in the gas phase but it becomes exothermic when system is solvated (Figure 10).

The stability of the ion–TATP complex is enhanced markedly if the cation is sandwiched between two TATP molecules. Such optimized complexes are shown in Figure 11 for  $\text{Cu}^{2+}$  and  $\text{H}_3\text{O}^+$ . The sandwich type complexes turn out to be much more stable than the ion–TATP complexes. In the case of  $\text{Cu}^{2+}$ , the ion leads to opening of the TATP ring when a single molecule participates in the complex, while in the TATP–ion–TATP case, both molecules in the complex have closed rings. It is also easy to see that, in the case of the hydronium ion, the nature of bonding is quite different between single and two TATP complexes. A more detailed comparison between a single and two TATP complexes with the different ions is shown in Table 1. The data clearly shows that formation of a sandwiched ion by two TATP molecules is much more stable than a complex with a single TATP. The increase in stability varies from one ion to another, but in most cases, we find a 30% increase or more. This pattern is true for both gas phase and solvated (i.e., THF) complexes. The only system for which a decreased stability is obtained is for the sandwich complex of  $\text{Cu}^{2+}$  in THF that is less stable than the  $\text{Cu}^{2+}$ –TATP complex. Inspection of Table 1 shows that, in all cases, the O–O and C–O distances in the sandwiched ions is shorter than that in the ion–single TATP complexes. Hence, the related bond energies in the sandwiched ions are larger and the corresponding transition state energies are expected to increase compared to the single TATP complexes. The higher stability of the sandwiched complexes together with the larger barriers for decomposition makes these species less favorable to be good initial candidates for TATP destruction. Consequently, the decomposition pathways of the sandwiched ions were not considered.

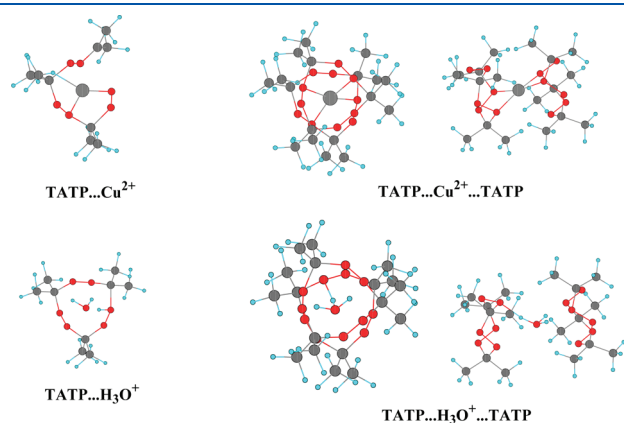


**Figure 11.** Optimized structures of ion–TATP (left column) and TATP–ion–TATP (right set of four pictures) complexes for  $\text{Cu}^{2+}$  and  $\text{H}_3\text{O}^+$ . In the case of sandwich-type complexes, the right column corresponds to the side view, while the left column corresponds to the top view.

**Table 1. Comparison of Geometries and Energetics of Single and Double TATP Complexes**

number of TATP molecules	binding energy		TS1		$R_{\max}(\text{O}-\text{O})$	$R_{\max}(\text{C}-\text{O})$	$R_{\min}(\text{Cat}-\text{O})$	
	gas phase	THF	gas phase	THF				
no ion			33.3	31.5	1.433	1.412	2.338	
$\text{Na}^+$	1-TATP	43.8	9.1	24.0	24.9	1.440	1.434	2.338
	2-TATP	73.6	17.9			1.439	1.429	2.457
$\text{Cu}^+$	1-TATP	66.2	36.2	22.6	20.3	1.442	1.445	2.156
	2-TATP	96.6	54.3			1.440	1.433	2.332
$\text{Cu}^{2+}$	1-TATP	264.5	136.1	13.6	17.1	1.448	1.560	1.984
	2-TATP	310.4	81.4			1.450	1.506	2.016
$\text{Zn}^{2+}$	1-TATP	218.2	105.5	15.2	16.9	1.453	1.497	1.987
	2-TATP	292.3	181.2			1.448	1.459	2.188
$\text{Co}^{2+}$	1-TATP	274.1	158.1	9.7	9.5	1.461	1.556	1.862
	2-TATP	351.1	200.3			1.456	1.514	1.972
$\text{H}_3\text{O}^+$	1-TATP	48.4	7.4	12.3	14.4	1.441	1.544	$\text{O}_{\text{TATP}}-\text{H}$ 1.001 and $\text{O}_{\text{H}_3\text{O}}-\text{H}$ 1.366
	2-TATP	68.9	17.1			1.440	1.456	$\text{O}_{\text{TATP}}-\text{H}$ 1.624 and $\text{O}_{\text{H}_3\text{O}}-\text{H}$ 1.023

**Table 2. Main Energetic Features of the Decomposition of Ion–TATP Complexes (Solvated)<sup>a</sup>**

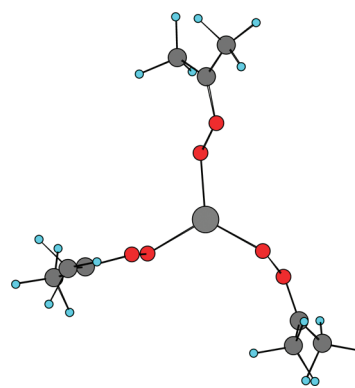
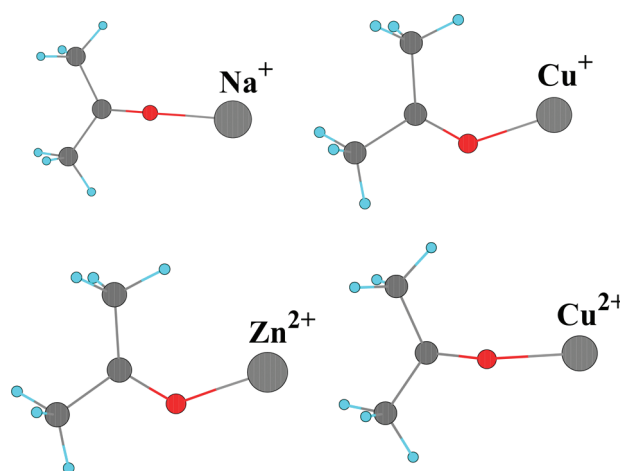
ion	complex stability	barrier height	energy release	energy release to separated products
no ion	0.0	36.3	−1.1	1.2
Cu <sup>1+</sup>	36.2	20.3	−35.4	−99.9
Na <sup>1+</sup>	9.1	27.2	−2.0	9.4
Cu <sup>2+</sup>	119.0 (132.4 <sup>b</sup> )	17.1	−35.0	20.9
Zn <sup>2+</sup>	105.5	16.9	1.0	12.7
Co <sup>2+</sup>	158.1	9.7	−88.4	−88.4
H <sub>3</sub> O <sup>1+</sup> (H <sup>1+</sup> )	7.4	14.4 (15.1)	−56.0 (−59.6)	−75.8

<sup>a</sup>The second column describes ion–TATP binding energy; third column, the main energy barrier for decomposition; fourth column, the energy release following TS structure relaxation; fifth column, the net energy release following decomposition products separation. All values correspond to solution in THF. Energy values in columns 3–5 are relative to the energy of ion–TATP in THF. Energy units are kcal/mol. <sup>b</sup>Stabilization energy for ion–TATP complex in which molecular ring is open.

#### IV. DISCUSSION AND CONCLUSIONS

If an explosive is diluted with a nonexplosive, its power is depleted. The exact amount of diluents required depends on the particular explosive/diluent considered. For example, commercial nitroglycerin is shipped 50% in acetone. TATP is a hydrophobic molecule, hence, its molecular crystal is poorly soluble in water. TATP destruction methods, published to date, involved the dissolution of TATP. The assumption was that the reaction is less violent with dilute TATP as discussed above. Ref 24 demonstrated effective TATP destruction in THF and ethanol acidic solutions of various metal ions. The enthalpy of TATP sublimation is 17.34 kcal/mol.<sup>38</sup> Moreover, electronic structure calculations suggest that the dissolution energy of TATP molecules in THF is practically zero. Because TATP dissolves well in THF, the entropy term has to be the driving force of the dissolution process. The magnitude of the sublimation entropy can be estimated from the pre-exponential term in the Arrhenius curve for TATP in ref 38 to be 62.4 cal mol<sup>−1</sup> K<sup>−1</sup>. Hence, at room temperature, the free energy of sublimation is approximately −2.0 kcal/mol and it increases for elevated temperatures. According to the results presented in Table 2, the formation of stable ion–TATP complexes reduces markedly the dissolution enthalpy. Hence, assuming only a small change in the entropy term, one expects that ion–TATP complex formation will increase the stability of the solution. The experiments suggest that a high ratio of ions to TATP molecules is required. This can be rationalized by moving the equilibrium to the solution of TATP complexed ions. A second possibility for the role of the ions is the weakening of the van der Waals forces by the strong salt effect. Furthermore, as will be discussed below, ion complexes may have an important role in the stabilization of TATP decomposition products.

Once the molecular crystal has dissolved, the second step is the decomposition of the ion–molecule complex in solution. Because the production of TATP is catalyzed by acids, a strongly acidic environment has been suggested and employed.<sup>24</sup> Metal ions are also known to catalyze the destruction.<sup>24,25</sup> The detailed mechanism of the ion–TATP decomposition process was the main interest in the present study. As already reported pre-

**Figure 12.** Minimum energy structure of the complex between Cr<sup>3+</sup> and the three acetone peroxides formed by TATP ring-opening.**Figure 13.** Structure of the complexes formed between acetone and the different ions.**Table 3. Binding Energies and Relative Stabilities of Various Ion–Acetone Complexes<sup>a</sup>**

	H <sub>3</sub> O <sup>+</sup>	Na <sup>+</sup>	Cu <sup>+</sup>	Cu <sup>2+</sup>	Zn <sup>2+</sup>	Co <sup>2+</sup>
R(O–ion) (Å)		2.123	1.881	1.909	1.873	1.834
ΔE <sup>b</sup> (gas phase)	26.9	36.1	54.5	188.4	149.9	212.4
ΔE <sup>b</sup> (THF)	5.8	12.1	34.6	109.4	86.2	137.7

<sup>a</sup>Energy units are kcal/mol. <sup>b</sup>ΔE = (E<sub>acetone</sub> + E<sub>cation</sub>) – E<sub>acetone·cation</sub>.

viously,<sup>25</sup> some ions form a complex with TATP without altering drastically the molecular structure, while other ions bind to TATP to form charged complexes while rupturing one or more molecular bonds during the complex formation. For the destruction of large TATP quantities, one would like to use the metal ions as catalysts in the destruction process. Otherwise, if the metal ions bond irreversibly to the TATP, vary large quantities of metal ion solutions will be required in the destruction process. Hence, metal ions that lead to the destruction of the TATP ring structure while forming highly stable complexes were not considered here. For this reason, we did not include in the present investigation ions such as Fe<sup>3+</sup> and Cr<sup>3+</sup> that spontaneously form highly stable charged complexes of the metal bound to three acetone peroxides, as shown in Figure 12 for Cr<sup>3+</sup>.

The initial steps of the complex decomposition process have common stages for all ions considered here. The first step in the process is to overcome an energy barrier associated with the rupture of a peroxide bond or a C–O bond. The magnitude of this energy barrier dictates the rate of the decomposition initiation. Once the system overcame this energy barrier, the rearrangement of the transition state geometry leads to an energy release. This energy release can lead to an efficient and rapid decomposition process. The next step along the decomposition path is the rupture of one or more additional bonds in the complex and its separation into decomposition products. The energy release and the separation into decomposition products stages may be separated by one or more transition states and intermediates that vary from one ion to another. A summary of the different energy values associated with the various decomposition steps studied here are presented in Table 2.

Inspection of the data in Table 2 shows that the stability of the TATP complex with singly charged ions is smaller by a factor of 3–12 than that of doubly charged ions. This significant stabilization energy of the  $\text{Cu}^{2+}$ –,  $\text{Co}^{2+}$ –, and  $\text{Zn}^{2+}$ –TATP complexes suggest that these ions may have an important role in the dissolution process of the TATP crystals. All ions examined in this study reduce markedly the magnitude of the main energy barrier that controls the initial decomposition step. It is clear that the three doubly charged ions and the hydronium ion lead to energy barriers that are less than half of that in the bare molecule. The decreased energy barriers are expected to result in a very large increase in the rate of the decomposition process.

However, an increased decomposition rate may lead to a violent autocatalytic reaction if it is highly exothermic. The fourth column in Table 2 shows that the hydronium ion as well as  $\text{Cu}^+$ ,  $\text{Cu}^{2+}$ , and  $\text{Co}^{2+}$  complexes with TATP lead to marked energy release, while initial steps along the decomposition path of  $\text{Zn}^{2+}$  are basically thermoneutral. Once final separated decomposition products are reached  $\text{Zn}^{2+}$ –TATP is also mildly exothermic. The large energy release together with relatively small energy barrier for decomposition in the case of  $\text{Co}^{2+}$ ,  $\text{Cu}^+$ , and  $\text{H}_3\text{O}^+$  can lead to detonation of the explosive when the destruction of large quantities are required. Experimental evidence related to TATP destruction with pure acids shows samples of gram size detonate, see discussion above. The relatively large energy barrier for initial decomposition in the case of  $\text{Na}^+$  is probably the reason why this ion did not show good decomposition ability in the experiments. To summarize, the analysis of the results obtained in the present study suggest that  $\text{Cu}^{2+}$  and  $\text{Zn}^{2+}$  are the two best candidates to be used in safe TATP destruction. This finding is in good agreement with the experimental data.

The requirement for high ion concentration in the solution (both metal ions as well as  $\text{H}^+$ ) may be related to an additional aspect, the stabilization of decomposition intermediates. In all decomposition routes discussed in this work, the first stable product formed is acetone. However, in most cases, additional nonstable intermediates are also obtained. Some of these intermediates are charged, due to the incorporation of the metal ion, but some are nonionic radicals. It is possible that existence of ions in the solution may stabilize these intermediates. For example, ions can form stable complexes through bonding to the oxygen end of the acetone molecule, hence, forming a stable ion–acetone complex. The structure of such complexes is shown in Figure 13. The ion–O distances together with the binding energies and relative stabilities of the various ion–acetone complexes are summarized in Table 3.

## ACKNOWLEDGMENT

Work supported by The Center of Excellence for Explosives Detection, Mitigation, and Response, Department of Homeland Security.

## REFERENCES

- (1) See for example: (a) McCullough, K. J.; Morgan, A. R.; Nonhebel, D. C.; Pauson, P. L.; White, G. J. *J. Chem. Res. Synop.* **1980**, 34–34. (b) McCullough, K. J.; Morgan, A. R.; Nonhebel, D. C.; Pauson, P. L. *Ibid.* **1980**, 36–37.
- (2) Adam, W.; Hadjiarapoglou, L. P.; Curci, R.; Mello, R. In *Organic Peroxides*; Ando, W., Ed.; John Wiley and Sons: Chichester, England, 1992; Chapt. 4.
- (3) Eyler, G. N.; Mateo, C. M.; Alvarez, E. E.; Canizo, A. I. *J. Org. Chem.* **2000**, *65*, 2319–2321.
- (4) Yavari, I.; Hosseini-Tabatabaei, M. R.; Nasiri, F. *J. Mol. Struct.* **2001**, *538*, 239–244.
- (5) Jubert, A. H.; Pis Diez, R.; Castro, E. A.; Canizo, A. I.; Cafferata, L. F. R. *J. Raman Spectrosc.* **1999**, *30*, 45–51.
- (6) Schaefer, W. P.; Fourkas, J. T.; Tiemann, B. G. *J. Am. Chem. Soc.* **1985**, *107*, 2461–2463.
- (7) Edward, J. T.; Chubb, F. L.; Gilson, D. F. R.; Hynes, R. C.; Sauriol, F.; Wiesenthal, A. *Can. J. Chem.* **1999**, *77*, 1057–1065.
- (8) Wierzbicki, A.; Cioffi, E. *J. Phys. Chem. A* **1999**, *103*, 8890–8894.
- (9) Wierzbicki, A.; Salter, E. A.; Cioffi, E.; Stevens, E. D. *J. Phys. Chem. A* **2001**, *105*, 8763–8768.
- (10) Schulte-Ladbeck, R.; Karst, U. *Anal. Chim. Acta* **2003**, *482*, 183–188.
- (11) Fialkov, A. B.; Gordin, A.; Amirav, A. *J. Chromatogr., A* **2003**, *991*, 217–240.
- (12) Schulte-Ladbeck, R.; Kolla, P.; Karst, U. *Anal. Chem.* **2003**, *75*, 731–735.
- (13) Oxley, J.; Zhang, J.; Smith, J. *Propellants, Explos., Pyrotech.* **2000**, *25*, 284–287.
- (14) Schulte-Ladbeck, R.; Kolla, P.; Karst, U. *Analyst* **2002**, *127*, 1152–1154.
- (15) Buttigieg, G. A.; Knight, A. K.; Denson, S.; Pommier, C.; Denton, M. B. *Forensic Sci. Int.* **2003**, *135*, 53–59.
- (16) Bellamy, A. J. *J. Forensic Sci.* **1999**, *44*, 603–608.
- (17) Hiyoshi, R. I.; Nakamura, J.; Brill, T. B. *Propellants, Explos., Pyrotech.* **2007**, *32*, 127–134.
- (18) Pachman, J.; Matyas, R. *Forensic Sci. Int.* **2010**, doi: 10.1016/j.forsciint.2010.10.010.
- (19) Eyler, G. N. *J. Phys. Org. Chem.* **2006**, *19*, 776–779.
- (20) Oxley, J. C.; Smith, J. L.; Chen, H. *Propellants, Explos., Pyrotech.* **2002**, *27*, 209–216.
- (21) Dubnikova, F.; Kosloff, R.; Almog, J.; Zeiri, Y.; Boese, R.; Itzhaky, H.; Alt, A.; Keinan, E. *J. Am. Chem. Soc.* **2005**, *127*, 1146–1159.
- (22) van Duin, A. C. T.; Zeiri, Y.; Dubnikova, F.; Kosloff, R.; Goddard, W. A. *J. Am. Chem. Soc.* **2005**, *127*, 11053–11062.
- (23) Oxley, J. C.; Smith, J. L.; Chen, H.; Cioffi, E. *Thermochim. Acta* **2002**, *388*, 215–225.
- (24) Oxley, J. C.; Smith, J. L.; Huang, J. R.; Luo, W. *J. Forensic Sci.* **2009**, *54*, 1029–1033.
- (25) Dubnikova, F.; Kosloff, R.; Zeiri, Y.; Karpas, Z. *J. Phys. Chem. A* **2002**, *106*, 4951–4956.
- (26) Cotte-Rodriguez, I.; Hernandez-Soto, H.; Chen, H.; Cooks, R. G. *Anal. Chem.* **2008**, *80*, 1512–1519.
- (27) Banerjee, S.; Mohapatra, S. K.; Misra, M.; Mishra, I. B. *Nanotechnology* **2009**, *20*, 1–6.
- (28) Frisch, M. J.; Trucks, G. W.; Schlegel, H. B.; Scuseria, G. E.; Robb, M. A.; Cheeseman, J. R.; Montgomery, J. A., Jr.; Vreven, T.; Kudin, K. N.; Burant, J. C.; Millam, J. M.; Iyengar, S. S.; Tomasi, J.; Barone, V.; Mennucci, B.; Cossi, M.; Scalmani, G.; Rega, N.; Petersson, G. A.; Nakatsuji, H.; Hada, M.; Ehara, M.; Toyota, K.; Fukuda, R.; Hasegawa, J.; Ishida, M.; Nakajima, T.; Honda, Y.; Kitao, O.; Nakai, H.

Klene, M.; Li, X.; Knox, J. E.; Hratchian, H. P.; Cross, J. B.; Bakken, V.; Adamo, C.; Jaramillo, J.; Gomperts, R.; Stratmann, R. E.; Yazyev, O.; Austin, A. J.; Cammi, R.; Pomelli, C.; Ochterski, J. W.; Ayala, P. Y.; Morokuma, K.; Voth, G. A.; Salvador, P.; Dannenberg, J. J.; Zakrzewski, V. G.; Dapprich, S.; Daniels, A. D.; Strain, M. C.; Farkas, O.; Malick, D. K.; Rabuck, A. D.; Raghavachari, K.; Foresman, J. B.; Ortiz, J. V.; Cui, Q.; Baboul, A. G.; Clifford, S.; Cioslowski, J.; Stefanov, B. B.; Liu, G.; Liashenko, A.; Piskorz, P.; Komaromi, I.; Martin, R. L.; Fox, D. J.; Keith, T.; Al-Laham, M. A.; Peng, C. Y.; Nanayakkara, A.; Challacombe, M.; Gill, P. M. W.; Johnson, B.; Chen, W.; Wong, M. W.; Gonzalez, C.; and Pople, J. A. *Gaussian 03*; Gaussian, Inc.: Wallingford, CT, 2004.

(29) Perdew, J. P.; Burke, K.; Ernzerhof, M. *Phys. Rev. Lett.* **1997**, *78*, 1396–1396.

(30) Adamo, C.; Barone, V. *J. Chem. Phys.* **1999**, *110*, 6158–6169.

(31) Dunning, T. H., Jr. *J. Chem. Phys.* **1989**, *90*, 1007–1009.

(32) Hurley, M. M.; Christiansen, P. A.; Ross, R. B.; Ermler, W. C. *J. Chem. Phys.* **1986**, *84*, 6158–6169.

(33) LaJohn, L. A.; Christiansen, P. A.; Ross, R. B.; Atashroo, T.; Ermler, W. C. *J. Chem. Phys.* **1987**, *87*, 2812–2824.

(34) Pacios, L. F.; Christiansen, P. A. *J. Chem. Phys.* **1985**, *82*, 2664–2671.

(35) Zhao, Y.; Truhlar, D. G. *Theor. Chem. Acc.* **2008**, *120*, 215–241.

(36) Barone, V.; Cossi, M. *J. Phys. Chem. A* **1998**, *102*, 1995–2001.

(37) Cossi, M.; Rega, N.; Scalmani, G.; Barone, V. *J. Comput. Chem.* **2003**, *24*, 669–681.

(38) Oxley, J. C.; Smith, J. L.; Luo, W.; Brady, J. *Propellants, Explos., Pyrotech* **2009**, *34*, 539–543.